ACTA MECHANICA SINICA (English Series), Vol.16, No.4, November 2000 ISSN 0567-7718
The Chinese Society of Theoretical and Applied Mechanics
Chinese Journal of Mechanics Press, Beijing, China
Allerton Press, INC., New York, U.S.A.

THE INVESTIGATION ON DYNAMIC FRACTURE BEHAVOUR OF MATERIALS UNDER COMPRESSIVE-SHEAR COMBINED STRESS WAVES*

Ma Wei (马 维) Duan Zhuping (段祝平)
(*LNM, Institute of Mechanics, CAS, Beijing* 100080, *China*)

ABSTRACT: In this paper, an improved plate impact experimental technique is presented for studying dynamic fracture mechanism of materials, under the conditions that the impacting loading is provided by a single pulse and the loading time is in the sub-microsecond range. The impacting tests are carried out on the pressure-shear gas gun. The loading rate achieved is $\mathrm{d}K/\mathrm{d}t \sim 10^8\,\mathrm{MPa\,m^{1/2}s^{-1}}$. With the elimination of influence of the specimen boundary, the plane strain state of a semi-infinite crack in an infinite elastic plate is used to simulate the deformation fields of crack tip. The single pulses are obtained by using the "momentum trap" technique. Therefore, the one-time actions of the single pulse are achieved by eradicating the stress waves reflected from the specimen boundary or diffracted from the crack surfaces. In the current study, some important phenomena have been observed. The special loading of the single pulse can bring about material damage around crack tip, and affect the material behavior, such as kinking and branching of the crack propagation. Failure mode transitions from mode I to mode II crack are observed under asymmetrical impact conditions. The mechanisms of the dynamic crack propagation are consistent with the damage failure model.

KEY WORDS: single pulse, compressive-shear combined stress wave, pressure-shear gas gun

1 INTRODUCTION

There are two kinds of dynamic fracture experiments of materials. One is carried out on conventional installations, such as the Kolsky bar, in order to investigate the dynamic responses of materials near crack tips under the loading conditions of low impacting velocities[1~9]. The loading rates achieved are $\mathrm{d}K/\mathrm{d}t \sim 10^{3\sim6}\,\mathrm{MPa\,m^{1/2}s^{-1}}$, and the loading duration of stress pulse is in microsecond ranges. At various loading rates, the cracking mechanisms of materials are brittle and/or ductile; the failure modes can be both of crack fracture and of adiabatic shear band; the transitions of failure modes and/or failure mechanisms, sometimes induced by unloading waves, are observed. The dynamic fracture toughness is very different from that under quasi-static loading. The micro-cracks around the crack tip may induce the propagating crack kink and branch. Owing to the limitation

Received 1 November 1999, revised 19 July 2000
* The project supported by the National Natural Science Foundation of China (No.19672066 and 18981180-4) and the Key Project of Chinese Academy of Sciences (No.KJ951-1-20)

of the present measuring technique and the influence of the boundary, it is impossible to study the mechanisms of the crack initiation and the stress wave diffracted from the crack surfaces in the tests.

However, tests can be conducted with the plate impact experiment carrying out on a pressure-shear gas gun[10,11]. The loading rates are approximately $\mathrm{d}K/\mathrm{d}t \sim 10^{8\sim9}\mathrm{MPa\,m^{\frac{1}{2}}\,s^{-1}}$. Because no unloading waves reach the crack tip during the loading, the plane strain state at the crack tip is obtained, which is similar to a semi-infinite crack tip in an infinite elastic plate. Upon impact, the compressive waves, which are reflected from the rear surface of the specimen and subject the crack tip to step tensile pulses inducing the initiation of crack, are generated. The impact speed and ambient temperature affect distinctly the mechanisms of the crack propagation. The time of the crack initiation can be fixed on experimental velocity-time profiles, which will be useful in studying the mechanisms of the crack propagation. But two problems involving the studies are:

1) Before the step tensile pulses arriving, the crack tip has already subjected to a compressive wave. The influence of the compressive wave on the material properties in the vicinity of the crack tip and on the mechanism of the crack initiation is still poorly understood.

2) After the crack initiation, the stress waves are reflected from the specimen boundaries and diffracted from the crack surfaces. It is necessary to study the influence of the phenomena on the mechanism of the crack propagation.

The objective of the present work is to probe into these problems. In Section 2 a description of the plate impact experimental technique is provided, which allows for the study of dynamic fracture processes when the impact loading is a single pulse and the loading time is in the sub-microsecond range. The improved plate impact experimental processes are described in Section 3. The experimental results are analyzed in Section 4. Lastly the conclusions of the present work are drawn.

2 EXPERIMENTAL PRINCIPLES

According to the theory of elastic waves[12] and combining with the experimental schemes of Refs. [2~4] and [10,11] shown in Fig.1 (a) and (b), a plate impact experiment is designed to load a mode II crack by an asymmetrical single pulse, which possesses the sub-microsecond time scales, and impinges at both normal (Fig.1(c)) and oblique incidence (Fig.1(d)). The diffracted wave pattern of the normal impact is shown in Fig.2(a) when the

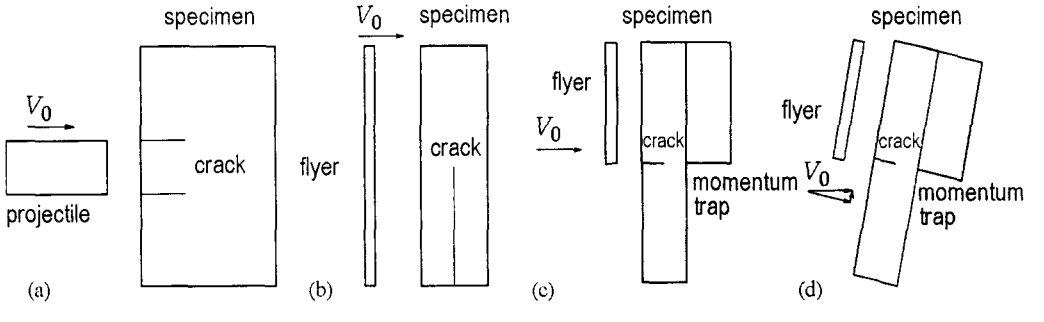

Fig.1 Experimental arrangements of Refs.[2~4] (a), [10,11] (b), and the present work (c), (d)

time interval is $t < 3l/c_d$, where l is the length of the crack and c_d is the elastic dilatational wave speed. Upon the impact, the dilatational plane wave ① propagating in the specimen is a step wave with the stress amplitude σ_0. At the same time, two cylindrical waves ② and ③, propagating at the dilatational wave speed c_d and the rotational wave speed c_s, respectively, are generated on the corner, A, of the crack line and the boundary of the specimen. The diffracted pattern includes the cylindrical wavefronts ④ and ⑤, when the dilatational waves, ① and ②, arrive at the crack tip simultaneously. Head waves ⑥ are also generated in order to satisfy the traction-free boundary conditions on the crack faces. In the same way, when the rotational wave ③ meets the crack tip, the cylindrical wave fronts ⑦ and ⑧ propagating at the dilatational and rotational wave speeds, and head waves ⑨ are generated. Figure 2(b) shows the diffracted wave pattern of the asymmetrical shear impact. The diffracted pattern of the asymmetrical oblique impact can be obtained by the superposition of the two situations.

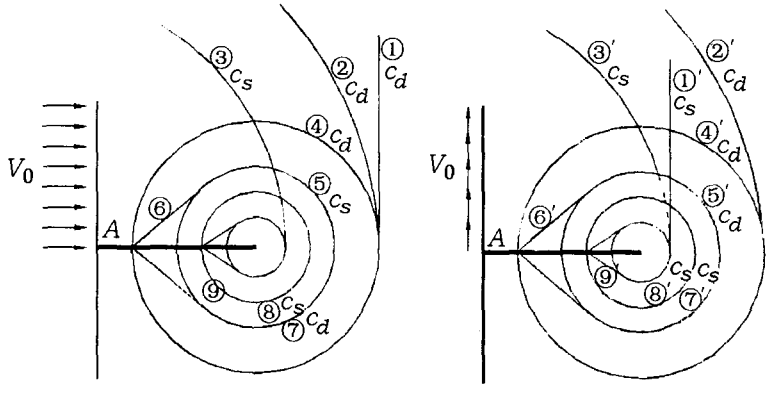

(a) (b)

Fig.2 Wavefronts for the diffraction of a plane wave by an edge crack under asymmetric normal (a) and oblique (b) impact loading, respectively

Under the asymmetrical impact conditions, a transient, mixed-mode deformation fields at the crack tip are induced, in which the mode II deformation field takes a large portion due to the main compressive wave, but a time-dependent mode I deformation field, which is only one seventh of the mode II component[13], is also generated. The dilatational pulse ① brings about the mode II deformation field at the crack tip in a normal impact. The compressive stress σ_0 can be measured directly by using Mn-Cu gages, or obtained by using the formulation in the elastic waves theory and the impact speeds measured,

$$\sigma_0 = \frac{\rho c_d V_0}{2} \tag{2.1}$$

where V_0, ρ are the impact velocity and the density of the material, respectively. The shear stress τ_0 can be determined based on the friction theorem, $\tau_0 = f_m \sigma_0$, where f_m is the friction coefficient of the material, which can be obtained by measuring the friction angle between the flyer and the specimen. The Poisson's effect of the compressive stress[14] and the plane rotational wave ①′ produce the mode I deformation field at the crack tip. The cylindrical waves ②$\sim$ ⑧, ②′$\sim$ ⑧′ lead to a mixed-mode deformation field at the crack tip.

The impact loading with a single pulse can be achieved by applying the "momentum trap" technique[15]. The time-distance diagram for the wave fronts, which traverse in the

elastic system consisting of the specimen, flyer and momentum trap, is shown in Fig.3. When the flyer impacts the specimen at time t_0, two compressive waves and two shear waves are generated, one compressive wave and one shear wave propagate in the specimen and the others propagate in the flyer. The compressive and shear waves that propagate in the flyer reach the rear surface at time t_1 and t_1', respectively, and are reflected from the rear surface as unloading waves. The compressive wave that passes through the specimen is reflected from the rear surface of the momentum trap as a tensile pulse at time t_2, and then propagates towards the specimen. Actually, the tensile stress appears in the system at the time t_3. When the tensile wave meets the interface PQ at time t_4, the interface fails, causing the momentum trap to separate. At this time, the unloading shear wave from the flyer has passed through the interface PQ, and reached the plane RS in the momentum trap. The thickness of the momentum trap is chosen such that the entire pulses are trapped. Thus, the large portion of the kinetic energy, produced by the flyer movement with a high impact speed, will become the kinetic energy in the momentum trap, and will not go back into the specimen. To this end, the flyer thickness required is less than a quarter of the specimen thickness or the momentum trap thickness, which are equal to each other. Therefore, the specimen is subjected to a single pulse of the known duration and amplitude and can be recovered entirely. It can also be proved that, if the ratio of the diameter to the thickness of the specimen is greater than four, the influence of the specimen boundary can be ignored, and the central part of the pre-notch in the specimen will be prevailed with a fully plane strain condition, which has been verified in the experiment[16].

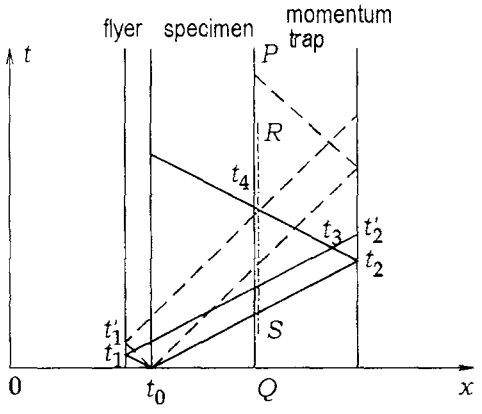

Fig.3 Time-distance diagram for the combined compressive-shear stress wave propagating in the flyer, specimen and momentum trap

3 EXPERIMENTAL PROCESSES

The material used for the studies is Hard C-60# steel with a diameter of 70 mm, of which the compositions and associated mechanical properties are given in Table 1. The Hard C-60# steel is chosen as the testing material for the reason that the material exhibits rate dependent fracture mechanisms, thus it would be suitable as a model material to examine the influence of loading rates on the microscopic and/or macroscopic behavior of materials in fracture processes. The material has been heat-treated normally: normalized at 880°C, and followed by rapid quenching in oil, then tempering at 200°C for 3 hours. The heat treatment has produced a relatively homogeneous microstructure, and reduced the size of the plastic deformed zone appearing near the advanced crack tip. The hardness of the material is around 52 HRC.

The specimen, flyer and momentum trap are produced with the same processes. The

Table 1 The composition and physical properties of 60# steel

C	Si	Mn	P	S	Cr	Ni
0.61	0.27	0.65	$\leq$0.04	$\leq$ 0.04	$\leq$ 0.25	$\leq$ 0.25

Heat treatment: normalized at 880°C followed by rapid oil quench, tempered at 200°C for 3 hours
Hardness: 52-54 HRC
Mass density: $\rho = 7800\,\mathrm{kg/m^3}$
Poisson's ratio: $\nu = 0.3$
Elastic Modulus: $E = 1.26\,\mathrm{GPa}$
Longitudinal wave speed: $C_d = 6020\,\mathrm{m/s}$
Shear wave speed: $C_s = 3220\,\mathrm{m/s}$
Rayleigh wave speed: $C_R = 2980\,\mathrm{m/s}$
Yield limit: $\sigma_s = 605\,\mathrm{MPa}$
Strength limit: $\sigma_b = 925\,\mathrm{MPa}$
Friction coefficient $f_m = 0.2$

Table 2 Summary of experiments on 60# steel

Shot No.	V_0 m/s	α °	P MPa	$\sigma_0^{1)}$ GPa	τ_0 GPa	$\sigma_{exp}^{2)}$ GPa	e_r %	Δl mm
01	181	0	1.5	3.67	0.00	3.81 (2.47)	3.9	0.10
02	173	0	1.5	3.46	0.00	3.71 (3.04)	7.1	0.11
03	183	0	1.5	3.71	0.00	3.69 (3.19)	0.4	0.09
04	192	15	1.5	3.76	0.90	3.48 (3.16)	7.4	0.10
05	187	0	1.5	3.79	0.00	3.94 (3.24)	4.1	0.07
06	184	15	1.5	3.60	0.86	3.65 (–)	1.5	0.10
07	204	15	1.0	3.99	0.96	– (3.58)	–	0.11
08	208	30	1.0	3.65	0.88	– (3.15)	–	0.11
09	156	15	0.3	3.05	0.73	– (2.89)	–	0.09

1) The results calculated according to the theory of elastic wave.

2) The results measured by using Mn-Cu compressive stress gages.

specimen is a circular disc of 45 mm in diameter and 10 mm in thickness. A notch of approximately 180μm in width and 5 mm in length is pre-machined through the thickness and diameter of the disc by electric discharge machining. Both the flyer and the momentum trap are in the shape of a semi-circular disc of 45 mm in diameter and 2.5 mm and 10 mm in thickness, respectively. The two surfaces of them are lapped flat to 2~3 Newton's rings over the diameter, and then are polished on Texmeth cloth over a flat plate, using a 3 μm diamond paste on a Lapmaster machine. The dimensions of them are shown in Fig.4. The specimen is so designed that no unloading waves would arrive at the crack tip from any circumferential part of the boundary in the interest time in the test, i.e. until the

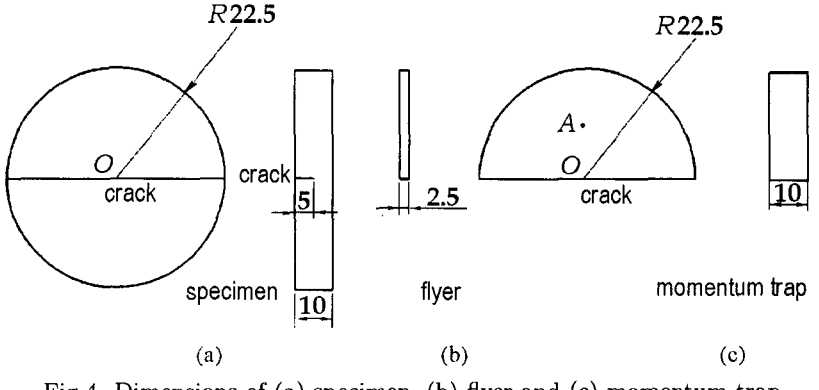

Fig.4 Dimensions of (a) specimen, (b) flyer and (c) momentum trap

unloading waves are reflected from the rear surface of the flyer that passes through the crack tip.

The impact tests are carried out on a pressure-shear gas gun (60 mm in diameter, 6 m long). Ordinarily, a longitudinal keyway in barrel prevents the axial rotation of the projectile, which makes it possible to carry out the two plate impact tests (Fig.1(a),(b)). Before the tests, the alignment is accurately completed[16]. The chamber is vacuum-pumped to a pressure less than $1.33 \times 10^{-2} \sim 9.33 \times 10^{-2}$Pa, and the parallel accuracy of impact faces is 0.01~0.08 mrad. During the impact, the pressures in the chamber are kept $2.66 \times 10^{-1} \sim 9.33 \times 10^{-1}$Pa, and the parallel accuracy of impact faces of the specimen and flyer is 0.04 mrad. The experimental gas is nitrogen, and the pressures are 1.5, 1.0 and 0.3 MPa, respectively.

The impact tests take place in a vacuum chamber at room temperature (Fig.5). A recovery technique[15] is used in order to recover the samples and evaluate the failure mechanisms by post-mortem microscope examinations of the fracture sample. The speed of the projectile is measured by the interruption of two pairs of probes placed across the path of the projectile. The speed ranges measured are 150~210 m/s, and the accuracy is in the range of 3 per cent. The compressive stresses are monitored by recording the voltage change of Mn-Cu stress gages in the interface of the sample, flyer and momentum trap. The microscopic mechanisms, such as, failure modes, fracture mechanisms, the damage initiation and damage evolution under a single stress pulse, are examined by observing the fracture surfaces using a scanning electron microscope.

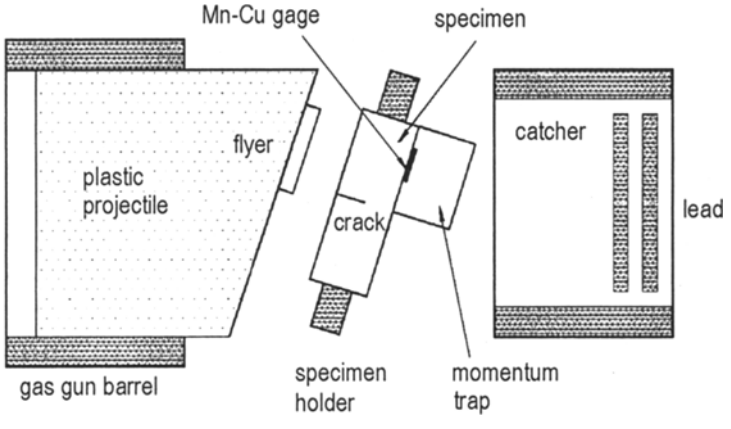

Fig.5 The experimental configuration

Under the loading conditions of a single pulse with sub-microsecond time scales, the crack initiation, propagation, arrest, the material damage and inelastic deformation occur in samples. In order to carry out the observation of the fracture surfaces and study the failure micro-mechanism with the scanning electron microscope, the sample is broken quasi-statically by the three-point bend tests on the Instron machine after the impact tests. During the processes the crack tips undergo a mode I deformation with loading rates of $dK/dt \sim 10^{1/2}\,\mathrm{MPa\,m^{1/2}s^{-1}}$.

4 EXPERIMENTAL RESULTS AND DISCUSSION

The experimental results are summarized in Table 2, which include the impact velocity

V_0, impact angle α, the calculated and measured compression stresses σ_0 and σ_{exp} (Fig.5) and their relative deviatives e_r, the shear stress τ_0 of the inclined impact, and the average crack growth Δl. The pressure values are about 3~4 GPa. The maximum compressive stress (4 GPa) reached in the tests corresponds to approximately 127% of the Hugniot elastic limit for the material. The average crack growth, which is about 100 μm, can be measured from the central region, 10~12 mm, of the notch front in the specimen. The impact speeds can be grouped into three ranges: high (200~220 m/s), medium (170~190 m/s) and low (160 m/s). Since a plastic deformed zone appears near the crack tip under the impact speed, the elasto-dynamic analytical solutions are in general not suitable for the field quantities near the crack tip, and the relative analysis of elasto-plasticity will be given in another paper. Here, we focus our attention only on the micro-mechanism analysis of the material failure mechanism in the dynamic fracture.

The compressive stress-time profiles measured by using stress gages are given in Fig.6 under impact conditions with different impact angles. The curves (a) and (b) in this figure correspond to the compressive stress-time profiles, which are measured by the gages of the impact surface of the specimen and the interface between the specimen and the momentum trap, respectively. The difference between the maximum amplitude of the two profiles is about 35%. The result testifies that a large energy carried with the stress pulse is diffused by some mechanisms, such as, material damage, crack initiation and heating due to deformation, taking place in the specimen. Two factors are responsible the fact that the pulse patterns are not ideal square waves. Firstly, the cohesive layer of the stress gages is too thick (0.1 mm) so that the rise time of the compressive wave front may delay about 200 ns. Secondly, the location of the stress gages is the area center of the half circle specimen, which is in the region where the unloading waves from the circumferential part of the boundary can arrive. Both the rise time delay and the influences of the boundary decrease with the magnitude of the pulse. However, it is not significant in comparison with the two compressive stress

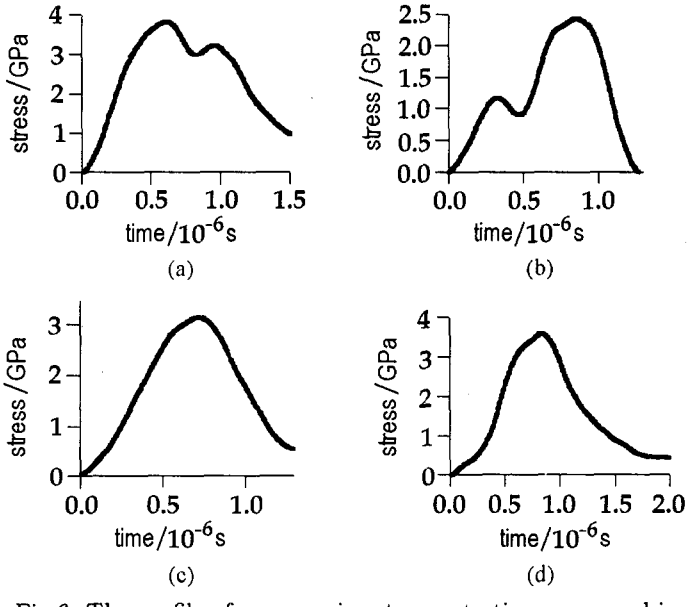

Fig.6 The profile of compressive stresses to time measured in Shot No.1 (a) and (b); Shot No.7 (c); Shot No.8 (d)

values, σ_0 and σ_{exp}. The maximum error between them is 7.4%, and the average error is 4.1%. If the stress gages are located at the center of a circle sample, the stress pulse profiles will be square waves, which are supported and reinforced by experimental results[16].

Figure 7 shows a fractographic picture of the fracture surface taken from the central region of specimen No.2. The crack growth in the region is found to be quite uniform. This fact supports the claim that a full plane strain state prevails in the central part of the specimen. Three distinct regions can be identified: (a) pre-notched region, (b) dynamic fracture region, and (c) static fracture region. The direction of the crack growth is from (a) to (b) then to (c). The region between (a) and (b) is the initial location of the crack, and the region between (b) and (c) is the arrest location. The extensive dimpling on dynamic fracture surfaces (Fig.8(a)) implies that a ductile failure mechanism is primarily operative. The material softening has occurred perhaps by the heating due to the plastic deformation. The driving force of the dynamic crack growth is the maximum shear stress along the crack line, which is the main reason for the ductile fracture. Figure 8(b) shows the quasi-static failure with the cleavage failure mechanism, which verifies that the 60# steel has become brittle after the heat treatment.

Fig.7 Dynamic crack growth in the central region of specimen No.2; $\alpha = 0°$, $V_0 = 173\,\mathrm{m/s}$

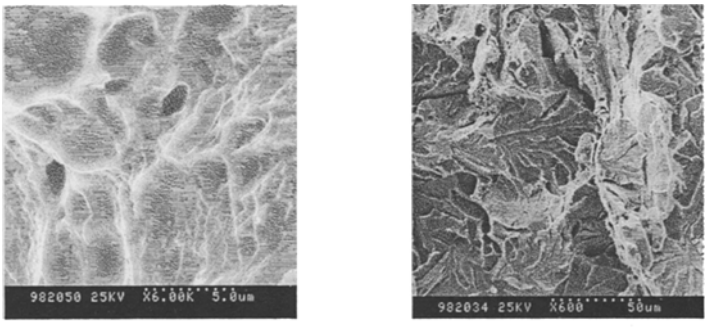

(a) (b)

Fig.8 Fractograph indicating (a) ductile fracture mechanism of dynamic crack growth; (b) cleavage fracture mechanism of quasi-static crack growth

Figure 9 shows the locations of the crack initiation on the periphery of the pre-notched tip under normal and oblique impacts. On both the normal impact and the inclined impact, the angle of the crack initiation is about 60°. This is because that the crack initiation is governed by the compressive stress pulse, and is independent of the shear wave. Clearly the

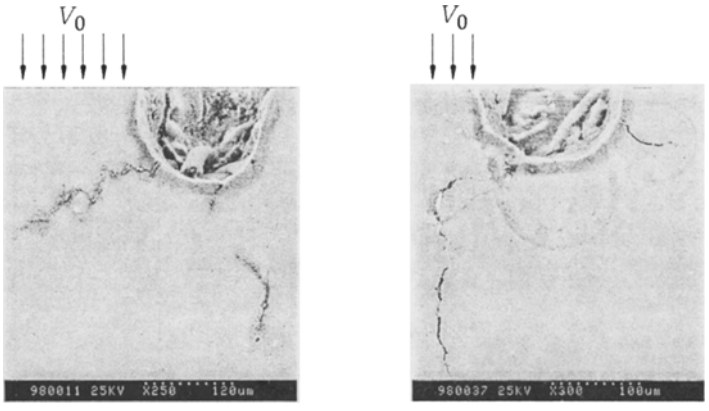

(a) normal impact (b) oblique impact

Fig.9 The locations of crack initiation on periphery of prenotch tip

crack initiation contributes to the stress concentration on the notched tip.

From Fig.9, a failure mode transition of the material from mode I crack to mode II crack is also observed under asymmetrical impact loading conditions. The crack growth consists of two phases. First, the crack initiation occurs on the impact periphery of the pre-notched tip, and the crack advances about 20 μm along the normal direction of the notch boundary in mode I crack growth, which shows that the maximum hoop stress criterion[17] probably governs the crack initiation. In this phase, the failure mechanism of I/II mixed-mode cracks dominates the mechanism of mode I crack growth. Second, the kink of the crack propagation occurs, that is, the crack growth changes its direction to that of the stress wave propagation or pre-notch line. The amplitude of the undulation of the fracture path is less then 15μm. The direction of the crack growth coincides with that of the maximum shear produced by the stress wave loading. The maximum shear stress criterion governs the crack growth, and the mechanism of the mixed-mode crack propagation behaves mainly as the mode II crack growth. This observation of the failure mode transition of the crack growth confirms the prediction of the idealized problem of the linear elasto-dynamic analyzed by Ref.[13]. The transition of the failure modes is responsible for the sub-microsecond single pulse and the pre-notch width[18]. It is observed that some secondary cracks emerge in the periphery of the pre-notch tip from Fig.9.

Unlike the studies[2~4,18], here only the crack fracture, but not the adiabatic shear band failure has been observed. The transition of both the failure modes between the crack fracture and the adiabatic shear band failure, and the failure mechanisms between brittle and ductile have not been observed, which are noticed in the investigations[1,2,18]. Under different loading conditions, the material failure modes depend on both the duration and the amplitude of the pulse. If the pulse duration is in the microsecond range and with a sufficient amplitude, the failure of the adiabatic shear band and the transitions of failure modes or failure mechanisms may occur. However, only the crack fracture mode will occur if the pulse duration is in the sub-microsecond range and with a short supply of energy. Therefore, the duration of the stress pulse is the decisive ingredient, which determines mainly the failure mode transitions from the crack fracture to the adiabatic shear band, and/or the failure mechanisms transitions from brittle to ductile.

The phenomenon, the so-called crack micro-branching, brought about by the micro-

cracks near the crack tips, is observed (Fig.10) to be different from the observations of the crack branching in the experiments[12,19]. In the present tests, the impact loading is a signal pulse with a large amplitude, which delays only $0.83\mu s$ for the normal impact tests and $2.28\mu s$ for the oblique impact tests. Such extreme conditions of impact loading induce sufficiently the micro-cracks inside the crack tip craze region to nucleate, grow and coalesce with cracks so as to form the crack micro-branching, but inactivate sufficiently the micro-crack outside the crack tip craze region to coalesce with cracks to form crack branching. Therefore the crack branching, which was observed by Ref.[9], is not observed in any of our experiments.

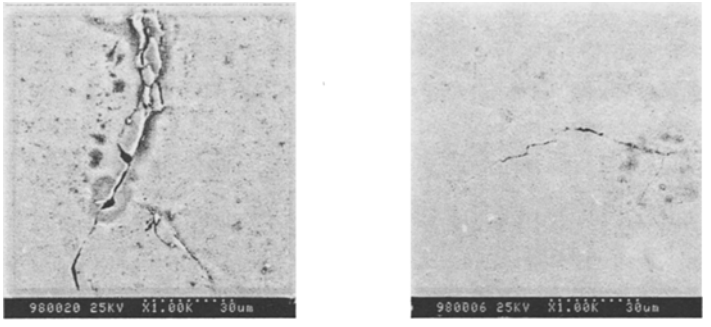

(a) (b)

Fig.10 The phenomena of crack micro-branching in tests No.1 and No.7

Figure 11 (a) is the fractograph picture of the pre-notched tip of specimen No.1. Many speckles like comets can be seen around the notch tip. From the magnified picture (Fig.11(b)) of these speckles, it can be identified readily that they are some micro-cracks and micro-voids. It is clear that the damage density near the tip is much higher than that far away from it, and the damage density is much higher on the loading side than on the non-loading side. The facts imply that a signal stress pulse can cause the material damage, and higher the amplitude of the stress is, the more serious the material damage will be. Therefore, a single compressive stress pulse will produce the material damage. The defects, such as micro-cracks and micro-voids, will cause the growth, branching and kinking of the crack, and accordingly the fracture follows the micro-crack fatigue model[19].

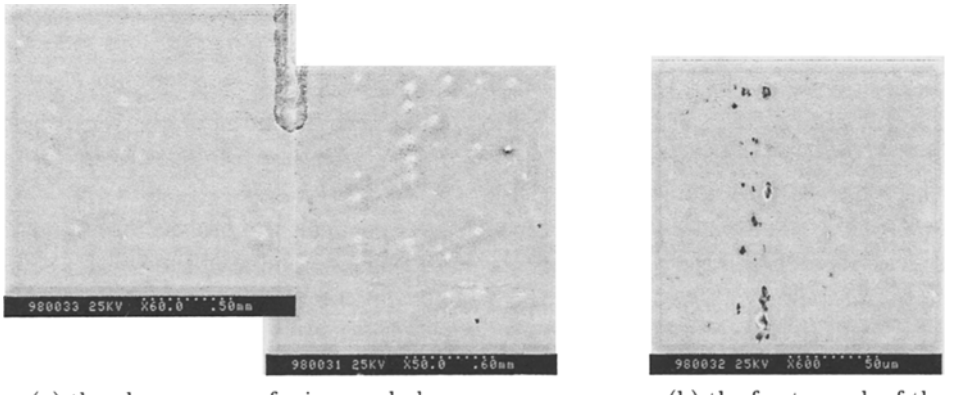

(a) the phenomenon of microcrack damage near notch tip induced by a signal-duration pulse

(b) the fractograph of the microcracks or voids near the notch tip

Fig.11

5 CONCLUSION

(1) An improved plate impact technique of studying material failure processes is proposed. Under asymmetrical impact loading conditions, the dynamic failure behavior of 60# steel exhibits the ductile mechanism due to the existence of the shear stress and the softening of the material occurs perhaps due to the heat resulting from the plastic deformation.

(2) Under a sub-microsecond single pulse only the fracture mode occurs, and the failure mode transition from mode I to mode II crack is observed. Both the failure behavior of the adiabatic shear band and the transition between it and the crack fracture have not been observed at present. The duration of the stress pulse is the decisive factor, which determines mainly the failure mode transitions from the crack fracture to the adiabatic shear band, and/or the failure mechanisms transitions from brittle to ductile. The phenomena of the stress pulse reflecting in the sample and diffracting on the crack tip many times may be another decisive factor. The amplitude of the stress pulse is a secondary factor.

(3) A single stress pulse can bring about a significant material damage. This material damage near the crack tip is considerably severe because of the phenomena of the stress concentration and high strain gradient. The nucleation, growth and coalescence of micro-cracks near the crack tip and their interaction induce the crack growth, kinking and branching. The dynamic crack propagation is consistent with the micro-crack damage model, which means that the micro-crack behavior near the crack tip governs the crack advance mechanism.

REFERENCES

1 Ravi-Chandar K. On the failure mode transitions in polycabnate under dynamic mixed-mode loading. *International Journal of the Solids and Structures*, 1995, 32(6/7): 925~938

2 Kalthoff J F. Shadow Optical Analysis of Dynamic Shear Fracture. Optical Engineering, 1988, 27: 127~133

3 Kalthoff J F. Transition in the failure behavior of dynamically shear loading cracks. *Appl Mech Rev*, 1990, 43(5) Part 2: S247~S250

4 Kalthoff J F, Winkler S. Failure mode transition at high loading. In: Proc Int Conf on Impact Loading and Dynamic Behaviour of Material. Cliem C Y, Kunze H D, Meyer L W, Eds. Bremen, May 18~22, 1987. Deutsche Gesellschaft fur Metallkunde, DGM, 1988. 185~196

5 Zhou M, Rosakis A J, Ravichandran G. Dynamically propagating shear bands in impact-loaded prenotched plates——I. Experimental investigation of temperature signatures and propagation speed. *Journal of the Mechanics and Physics of Solids*, 1996, 44(6): 981~1006

6 Ravi-Chandar K, Knauss W G. An experimental investigation into dynamic fracture: I. Crack initiation and arrest. *International Journal of Fracture*, 1984, 25: 247~262

7 Ravi-Chandar K, Knauss W G. An experimental investigation into dynamic fracture: II. Microstrutural aspects. *International Journal of Fracture*, 1984, 26: 65~80

8 Ravi-Chandar K, Knauss W G. An experimental investigation into dynamic fracture: III. Steay-state crack propagation and crack branching. *International Journal of Fracture*, 1984, 26: 141~154

9 Ravi-Chandar K, Knauss W G. An experimental investigation into dynamic fracture: IV. On the interaction of stress wave with propagating cracks. *International Journal of Fracture*, 1984, 26: 189~200

10 Ravichandran G, Clifton R J. Dynamic fracture under plane wave loading. *International Journal*

of Fracture, 1989, 40: 157~201

11 Prakash V, Clifton R J. Experiment and Analytical Investigation of Dynamic Fracture under Conditions of Plane Strain. In: Ernst H A, Saxena A, McDowell D L, Eds. Fracture Mechanics: Twenty-Second Symposium. Vol. I, ASTM STP 1131.
American Society for Testing and Material, Philadelphia, 1992. 412~444

12 Wang Lili, Zhu Zhaoxiang. The Foundation of Stress Wave. Beijing: National Defense Industry Publication, 1985. 36

13 Lee Y J, Freund L B. Fracture initiation to asymmetric impact loading of an edge craked plate. *Journal of Applied Mechanics*, 1991, 57: 104~111

14 Freund L B. Dynamic Fracture Mechanics. NY: Cambridge University Press, 1990

15 Kumar P, Clifton R J. Dislocation Motion and Generation in Single Crystals Subjected to Plate Impact. *J Appl Phys*, 1990, 50: 4747

16 Ma Wei. Experimental and theoretical studies on the dynamic fracture toughness of materials under pressure-shear combined stress waves. Ph D thesis. Institute of Mechanics of CAS, 1998

17 Erdogan F, Sih G C. On the crack extension in plates under plane loading and transverse shear. *Journal of Basic Engineering*, 1963, 85D: 519~527

18 Zhou M, Rosakis A J, Ravichandran G. Dynamically propagating shear bands in impact-loaded prenotched plates——I. Experimental investigation of temperature signatures and propagation speed. *Journal of the Mechanics and Physics of Solids*, 1996, 44(6): 981~1006

19 Cotterell B. Fracture propagation in organic glasses. *International Journal of Fracture*, 1968, 4: 209